



HAL
open science

Low Temperature Silicon Oxide Deposition on Polymer Powders in a Fluidized Bed Coupled to a Cold Remote Plasma

Hubert Caquineau, Lynda Aiche, Hugues Vergnes, Bernard Despax, Brigitte Caussat

► **To cite this version:**

Hubert Caquineau, Lynda Aiche, Hugues Vergnes, Bernard Despax, Brigitte Caussat. Low Temperature Silicon Oxide Deposition on Polymer Powders in a Fluidized Bed Coupled to a Cold Remote Plasma. *Surface and Coatings Technology*, 2012, 206 (23), pp.4814-4821. 10.1016/j.surfcoat.2012.04.091 . hal-03468980

HAL Id: hal-03468980

<https://hal.science/hal-03468980>

Submitted on 7 Dec 2021

HAL is a multi-disciplinary open access archive for the deposit and dissemination of scientific research documents, whether they are published or not. The documents may come from teaching and research institutions in France or abroad, or from public or private research centers.

L'archive ouverte pluridisciplinaire **HAL**, est destinée au dépôt et à la diffusion de documents scientifiques de niveau recherche, publiés ou non, émanant des établissements d'enseignement et de recherche français ou étrangers, des laboratoires publics ou privés.



Open Archive Toulouse Archive Ouverte (OATAO)

OATAO is an open access repository that collects the work of Toulouse researchers and makes it freely available over the web where possible.

This is an author-deposited version published in: <http://oatao.univ-toulouse.fr/>
Eprints ID: 6139

To link to this article: DOI:10.1016/j.surfcoat.2012.04.091
<http://dx.doi.org/10.1016/j.surfcoat.2012.04.091>

To cite this version:

Caquineau, Hubert and Aiche, Lynda and Vergnes, Hugues and Despax, Bernard and Caussat, Brigitte *Low Temperature Silicon Oxide Deposition on Polymer Powders in a Fluidized Bed Coupled to a Cold Remote Plasma*. (2012) *Surface and Coatings Technology*, vol. 206 (n° 23). pp. 4814-4821. ISSN 0257-8972

Any correspondence concerning this service should be sent to the repository administrator: staff-oatao@inp-toulouse.fr

Low temperature silicon oxide deposition on polymer powders in a fluidized bed coupled to a cold remote plasma

H. Caquineau^{a,b,*}, L. Aiche^{a,b,c,1}, H. Vergnes^c, B. Despax^{a,b}, B. Caussat^c

^a LAPLACE (Laboratoire Plasma et Conversion d'Energie), Université de Toulouse, UPS, INPT, 118 route de Narbonne, F-31062 Toulouse Cedex 9, France

^b LAPLACE, CNRS, 118 route de Narbonne, F-31062 Toulouse, France

^c Laboratoire de Génie Chimique, UMR CNRS 5503, ENSIACET/INPT, 4, allée Emile Monso, BP 84234, 31432 Toulouse Cedex 4, France

A B S T R A C T

In this work silicon oxide has been deposited from silane on fluidized polyethylene powders placed in a far cold remote nitrogen/oxygen plasma. The process temperature remained below 100 °C. The influence on the powder wettability of several key parameters such as the amount of oxygen injected in the plasma, the SiH₄ flow rate and the treatment duration has been studied. From hydrophobic, the polyethylene powder wettability can be drastically improved depending on process conditions. Based on surface analyses of treated powders under various processing conditions, a deposition mechanism has been proposed combining homogeneous and heterogeneous nucleation and growth phenomena. The observed wettability variations appear to be linked to the surface coverage of the powder by the deposit.

Keywords:

Plasma assisted deposition
Fluidized bed
Powder
Wettability
Polyethylene
Silicon oxide

1. Introduction

Cold plasma technologies are extensively used in the industry in order to change the surface of materials without affecting their intrinsic bulk properties. The resulting modifications of the surface properties are either due to a change of the chemical moieties at the surface or to the deposition of a thin film. This widespread use of cold plasma technologies is a consequence of the opportunity they offer to create highly-active chemical species in a gas without any substantial temperature increase [1]. Nevertheless, although plasma technologies are commonly used for modifying plane substrates, treating non-planar materials is much less usual. As 50% of the material used in the industry is in the form of powder [2], this can be considered as a major drawback of plasma processes. Different technologies of reactors can be used: mechanically-stirred powder reactors [3,4], fluidized bed reactors [5–7], circulating fluidized bed reactors [8], gravity and downer reactors [9,10]. In the present work, the active gas was put in contact with the powders in a fluidized bed (FB). FB generates intense thermal and mass transfers between gas and particles, and thus leads to very uniform treatments.

Nevertheless, as underlined by Karches et al. [11], a major drawback of putting together in contact a cold plasma and particles is the resulting heating (formation of hot points), which is unacceptable for thermally sensitive materials. An interesting way to overcome this impediment has been developed by Mutel et al. [12,13]: the fluidized bed is placed 0.65 m downstream a microwave nitrogen discharge. This allows avoiding the contact between the plasma energetic species (electrons, ions, etc.) and the powders which is responsible for the powder bed overheating. However, this cannot be achieved with any gas. Nitrogen-plasmas generate long-living chemically active species, mainly atomic nitrogen and metastable species, and so, active post-discharges [14].

Modifying the surface properties of polymer powders is interesting because polymer powders are widely used in the industry as raw material. Since polymers are temperature-sensitive materials, low temperature plasma assisted processes are appropriate tool to perform such modification [15]. Just to quote a few examples of plasma-assisted treatment of polymer powders, the powders, generally made of polyethylene (PE), can be fluorinated in order to give them a Teflon-like surface with the corresponding properties of chemical inertness, low surface energy and thermal energy storage capability [16,17]. Amine moieties can also be grafted on the powder surface for biotechnological applications [7]. In the literature, plasma-assisted processes are mainly used to change the surface property of polymer powder from hydrophobic to hydrophilic [6,12,13,18–20]. That allows obtaining water-based stable slurries in industries such as paintings, textile and that could also be a way to develop new composite materials. In a previous article [21],

* Corresponding author at: LAPLACE (Laboratoire Plasma et Conversion d'Energie), Université de Toulouse, UPS, INPT, 118 route de Narbonne, F-31062 Toulouse Cedex 9, France. Tel.: +33 5 61 55 84 53; fax: +33 5 61 55 64 52.

E-mail addresses: caquineau@laplace.univ-tlse.fr (H. Caquineau), Hugues.Vergnes@ensiacet.fr (H. Vergnes), despax@laplace.univ-tlse.fr (B. Despax), Brigitte.Caussat@ensiacet.fr (B. Caussat).

¹ Co-first author.

polyethylene powders were functionalized in nitrogen post-discharges with or without oxygen addition. Nevertheless, the improved wettability which is obtained after a nitrogen or an oxygen plasma treatment does not last very long and generally after a few days, the wettability is close to that of the non-treated powder [19]. The present paper focuses on silicon oxide deposition on polyethylene powders from silane (SiH₄) and oxygen in nitrogen post-discharges at temperatures lower than 100 °C. Covering the powder with such a coating should lead to long-lasting effects on the powder wettability.

The influence of some key operating parameters such as the oxygen and SiH₄ flow rates, the mass of powder and the treatment duration on the characteristics of the deposit was studied. The particles wettability was evaluated through contact angle measurements. The deposit chemical composition was analyzed by Attenuated Total Reflectance Fourier Transform Infra-Red (ATR FT-IR) spectroscopy and by Inductively Coupled Plasma Chemical Analysis (ICP-CA). The coverage of the powder surface and its morphology were studied by Field Effect Gun Scanning Electron Microscopy (FEG SEM) and by Energy-Dispersive X-ray spectroscopy (EDX). The post-discharge was analyzed by Optical Emission Spectroscopy (OES). In the following section of this paper, the experimental setup, the studied powders and the characterization methods are described. Then, the main results obtained are presented and discussed.

2. Experimental

2.1. Experimental set-up and conditions

The experimental set-up is presented in Fig. 1. Experiments were carried out in a fluidization glass column, 0.05 m in diameter and 0.9 m in height. High density polyethylene (PE) powders (ICOPOLYMER, icorene 1339), 260 µm in Sauter diameter and 930 kg.m⁻³ in grain density, have been studied. The particles were fluidized by a mixture of nitrogen and oxygen gasses (respectively N50 and Alpha quality, Air Liquide). Gas flow-rates were regulated by mass flow controllers. The particles were supported by a gas-distributor designed in our lab as discussed later on. The total pressure in the fluidization column was maintained at 10 Torr by means of a vacuum pump and a vacuum regulation valve. For each experiment, the leak rate was below 0.2 Torr.L.min⁻¹. The reactor pressure was measured at the top of the column by a Baratron vacuum gauge. The gauge can also be connected below the gas distributor in order to calculate the fluidized bed pressure drop. Elutriated particles, i.e. particles lost in the exhaust line, were captured by a particle filter.

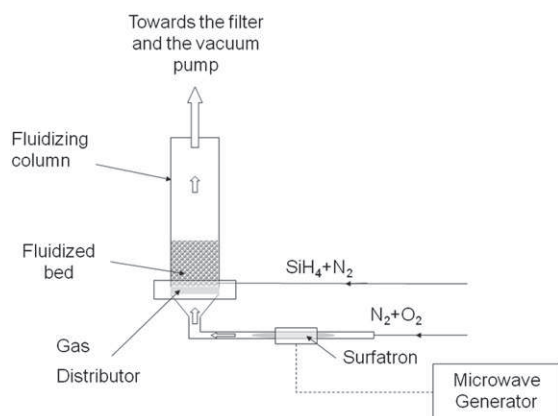


Fig. 1. Experimental set-up.

The fluidizing gas mixture (N₂ or N₂ + O₂) was excited by flowing in a quartz tube (inner diameter 9 mm) through a microwave cavity (surfatron) powered by a microwave generator (2450 MHz) which can deliver up to 300 W. This tube was connected to the bottom of the fluidized bed reactor. The microwave cavity was placed 47 cm upstream the gas distributor which supports the bed. The temperature measured just above the gas distributor by a thermocouple never exceeded 100 °C.

Silane (diluted up to 2.5 vol.% in nitrogen) was injected directly in the fluidized bed through an annular injector located at 2 cm above the distributor.

The nominal mass of PE powders treated in this reactor was 51 g. This corresponds to a fixed bed height of 5 cm and to a ratio of the fixed bed height over the fluidization column inner diameter of 1. The tested operating conditions are given in Table 1. The reference run is S5. For the other runs, only one parameter was varied with respect to S5.

In order to remove organic contaminants and to improve the adhesion of silicon oxide on the powder polymeric surface [22,23], the PE powders were systematically fluidized in the reactor for 1 h under 10 Torr in a post-discharge composed of nitrogen and oxygen (0.3 vol.% of O₂, total flow rate of 800 sccm, power of 300 W) just before each deposition run.

The post-discharge characteristics were studied by OES measurements performed at 4 cm below the distributor using a GetSpec 2048 (Sentronic) spectrometer.

The water contact-angle of the treated PE powders was obtained by means of a GBX Tensiometer and using the Washburn's method [24]. 500 µg of PE powders were packed into a glass column (10 mm ID), whose bottom is closed with a porous sieve. The glass column was then put in close contact with water that penetrated up in the PE powders column by capillarity rising. The weight of penetrating water was measured as a function of time. The contact angle of the PE powder surface is then governed by the modified Washburn equation: [24]

$$\frac{m^2}{t} = C\rho_l^2\sigma_l \frac{\cos\theta}{\eta_l} \quad (1)$$

where η_l (Pa.s), ρ_l (kg.m⁻³) and σ_l (mN.m⁻¹) are respectively the viscosity, density and total surface tension of the chosen liquid. C is a constant which is determined from measurements done with a liquid that perfectly wets the powder (heptane in our case). The contact angles presented in the present paper correspond to an average of three measurements. The maximum deviation from the mean value is $\pm 2.5^\circ$. This low deviation between measurements carried out on different samples from the same run shows the uniformity of the treatment over the whole bed. The water contact angle of the non-treated PE powders is higher than 90°.

Table 1

Operating conditions (sccm: cm³.min⁻¹ in standard conditions of temperature and pressure). The total N₂/O₂ flow-rate through the surfatron is always 640 sccm and the total N₂/SiH₄ flow-rate through the annular distributor is always 160 sccm.

Run	O ₂ flow rate (sccm)	Vol.% of O ₂	Silane flow rate (sccm)	Deposition duration (hours)	Mass of powders (g)
S1	0.00	0	4	2	51
S2	0.15	0.02	4	2	51
S3	0.63	0.09	4	2	51
S4	2.20	0.34	4	2	51
S5	3.00	0.47	4	2	51
S6	3.00	0.47	0	2	51
S7	3.00	0.47	2	2	51
S8	3.00	0.47	4	1	51
S9	3.00	0.47	4	2	25
S10	3.00	0.47	4	2	100

The chemical modifications of the powders surface were characterized by attenuated total multiple reflection infra-red spectrometry (ATR FT-IR) using a Nicolet 5700 spectrometer. A diamond prism was used and the incident angle of the IR radiation was 45°.

The morphology of the treated powders surface was analyzed using a Jeol JSM 6700F FEG SEM microscope. EDX analyses were performed in the same apparatus. The samples were stuck onto copper mounts using a conducting silver paint. As PE is an insulating material, the samples were coated by a very thin Pt layer in a sputtering device in order to avoid charge effects. EDX spectra were obtained with a low beam voltage of 5 kV in order to minimize the beam depth penetration. With a voltage of 10 kV, the signal due to the deposit became very low compared to that of the PE powders.

The global weight percentage of silicon deposited on powder samples was measured by a Thermo-Fisher iCAP6300 inductively coupled plasma spectrometer (ICPS).

After each run, the powders were stocked in closed PE bottle at ambient temperature in air.

2.2. The far cold nitrogen remote plasma in the experimental context

Nitrogen post-discharges are widely described in the literature. A nitrogen discharge can give rise to a significant post-discharge depending on the operating conditions (pressure, nitrogen purity, etc.). This post-discharge can be divided into three main zones when going from the discharge to downstream: an intermediate zone, a secondary ionization zone (also known as the pink afterglow) and the far cold remote nitrogen plasma (FCRNP), also known as the yellow afterglow [25]. The nitrogen post-discharge is mainly the result of the creation in the discharge itself of an energy reservoir which is constituted by (i) vibrationally excited nitrogen molecules in their ground state : N_{2v} , and (ii) metastable molecules: $N_2(A)$ and $N_2(a')$ [14]. In this work, the fluidized bed is placed in the FCRNP, since it is a low temperature zone. The main active species in this zone are the nitrogen radicals in their ground-state $N(^4S)$, N_{2v} and $N_2(A)$. The extension of the yellow post-discharge results from the following chain mechanism:



In the third reaction (R3), $N_2(A)$ dissociation back to $N(^4S)$ is due to the presence of N_2 in energetic metastable states. The emission at 580.43 nm resulting from the $N_2(B)$ to $N_2(A)$ transition is characteristic of the FCRNP [26]. Moreover, the optical emission intensity at this wavelength is proportional to $[N(^4S)]^2$ [27]. Hence, following this intensity is a good means to appreciate the yellow FCRNP activity.

Working in the FCRNP has important consequences on the experimental set-up. On one hand, the microwave cavity should not be too close to the bed in order to avoid the contact of too energetic species with the distributor and the fluidized bed, i.e. precisely in order to work at a low temperature in the FCRNP. On the other hand, it should not be too far from the bed in order to maximize the concentration of active species in the fluidized bed. Finding a compromise between those two opposite requirements is all the more difficult as the transmission of active species through the gas distributor below the bed plays a major role. In order to overcome the high loss probability of $N(^4S)$ species on metals [28] and the modification of the post-discharge resulting from its contact with

polymers [29], a special distributor was designed for this work. In this distributor, the FCRNP is only in contact with silica.

2.3. PE powders fluidization

The choice to work under 10 Torr resulted from a compromise between plasma and fluidization requirements: the fluidization quality gets poorer when the pressure decreases [30], whereas the concentration of the plasma-induced active species tends to decrease drastically above 10 Torr as evidenced by OES measurements [31].

By using the Davidson and Harrison method [32], the pressure drop curve, shown in Fig. 2, was determined under 10 Torr at decreasing gas flow rate using pure nitrogen at ambient temperature. The normalized differential pressure drop ΔP^* was obtained by dividing the measured differential pressure across the bed by the theoretical one, which is equal to the bed weight per unit column area. The abscissa corresponds to the superficial gas velocity U , i.e. the gas velocity in the empty column in conditions of Standard Temperature and Pressure (STP). First, a plateau is clearly visible beyond 0.2 cm.s^{-1} , proving that the bed of PE particles is well fluidized. The minimum fluidization velocity U_{mf} was deduced from the intersection of the two asymptotes, as being about 0.07 cm.s^{-1} STP (i. e. 5.3 cm.s^{-1} under 10 Torr). This is a rough value since the transition from the ascending part of the curve to the plateau is not abrupt. Indeed under reduced pressure, a bed of particles progressively enters in fluidization from its top part to its bottom part, i.e. there is a range of minimum fluidization velocities, a beginning one and a finishing one, which corresponds to the fluidization of the whole bed particles [33]. In our case, this range of minimum fluidization velocities has never been evidenced visually in our column and we verified that below U_{mf} , the bed was fixed. This U_{mf} value agrees with that predicted by the correlation of Llop et al. [30] which is about 4 cm.s^{-1} under 10 Torr.

The injection of silane just above the gas distributor and the plasma ignition showed no appreciable influence on the fluidization quality.

For all runs, we chose to work at a fluidization ratio (U/U_{mf}) close to 9. Then, the N_2 and O_2 total flow rate through the surfatron is 640 sccm. Under this condition, a convenient hydrodynamics of bubbling bed was obtained and the expanded bed height was 10 cm for 51 g of particles. This rather high flow rate ensured a good yellow post-discharge transmission through the distributor: without bed, the yellow post-discharge filled the fluidization column. The elutriation for 3 h of fluidization was less than 10% of the initial bed weight. According to specific measurements, it mainly occurs during the first 30 min [31].

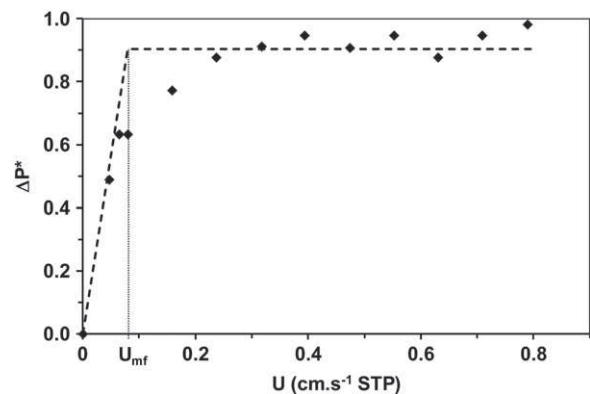


Fig. 2. Normalized differential pressure drop across the bed versus decreasing nitrogen velocity at ambient temperature and at 10 Torr. All the gas was flowing through the gas distributor.

3. Results and discussion

3.1. Wettability and OES results

The influences on the powder wettability of the oxygen flow rate, the silane flow rate, the deposition duration and the bed mass were studied for the operating conditions of Table 1. The water contact angle evolution with the oxygen flow rate and other parameters kept at a constant value (runs S1 to S5) are represented in Fig. 3 and the water contact angle is given for the runs S6 to S10 corresponding to a constant O₂ flow rate of 3 sccm in Table 2. Optical emission measurements (not given) showed no appreciable differences from one run to another in Table 2 meaning that the variations of the contact angle in Table 2 are not caused by changes in the discharge and post-discharge characteristics. Since the crude powder is hydrophobic, the contact angle can be seen as a good indicator of the surface modification. In a previous paper [21], treating identical PE powders with pure nitrogen post-discharge did not affect their water contact angle. When adding oxygen up to 1 vol.% to the discharge, the water contact angle only dropped to 65°. Then, the important lowering of the water contact angle showed in Fig. 3 and Table 2 is the result of the deposition of a silicon-containing coating on the powder.

3.2. Process efficiency

The evolution of the contact angle as a function of the mass of treated powders shows a minimum for 51 g (runs S5, S9 and S10 in Table 2). This gives information on the optimal use of the post-discharge active species in the fluidized bed. Indeed, the concentration of these species decreases when penetrating the fluidized bed because of their consumption by reactions with silane as well as with the powder surface. Therefore, there is an optimal bed height beyond which the concentration of active species becomes too low to substantially modify the powder surface. If the fluidized bed is higher than this height, the process becomes less efficient. This is confirmed by the fact that the 100 g batch yields to a lesser wettability improvement than the 50 g batch. As silane is injected 2 cm above the gas distributor, the bottom part of the bed is mostly inefficient because the global gas flow goes upward. Consequently, the 25 g bed (fixed-bed height of 2.5 cm) gives worse results than the 51 g bed.

In terms of silane conversion, the mass of silicon deposited on powders measured by ICPA is 0.18 ± 0.01 g in the case of run S5. This corresponds to 31 atomic percentage of the entering silicon. Another part of the entering silicon is converted either in deposit on column wall or in dust particles which stick on the glass column or are elutriated. This implies that homogeneous (i.e. in the gas phase) mechanisms of particle nucleation and growth exist in this

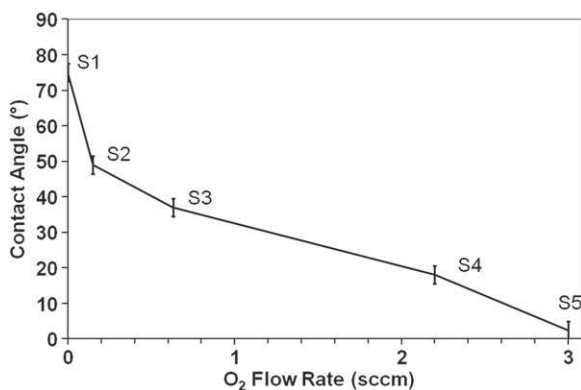


Fig. 3. Variation of the water contact angle as a function of oxygen flow rate.

Table 2

Water contact angles measured after runs S6 to S10. For each run, the parameter which differs from the reference run (S5) is given in the second column.

Run	Studied parameter (in comparison with run S5)	Contact angle
S5	–	<5°
S6	Silane flow-rate (0 sccm vs. 4 sccm in run S5)	82°
S7	Silane flow-rate (2 sccm vs. 4 sccm in run S5)	42.5°
S8	Run duration (1 h vs. 2 h in run S5)	47°
S9	Bed mass (25 g vs. 51 g in run S5)	49°
S10	Bed mass (100 g vs. 51 g in run S5)	54°

process. The creation of dusts is a well-known phenomenon in deposition plasmas [34].

3.3. Influence of the oxygen flow rate

Adding oxygen to the nitrogen flowing through the discharge zone modifies the nature of the deposit, as it will be discussed later, but, it also induces important effects on the post-discharge. Indeed, although oxygen is known to quench vibrationally and electronically-excited nitrogen molecules [35], it was reported that when adding very low oxygen concentration, i.e. typically below 1 vol.%, the N(⁴S) concentration increases in the nitrogen post-discharge [36,37]. The reasons for this enhancement are still unclear as discussed by Mrazkova et al. [38]. The 580.43 nm emission measured just below the gas distributor is presented as a function of the oxygen vol.% in Fig. 4 at a total flow rate of 640 sccm. It can be observed that adding as low O₂ concentrations as 0.02 vol.% O₂ to N₂ results in a drastic increase of the 580.43 nm intensity and so of the N(⁴S) concentration. Adding oxygen from 0.02 up to 0.47 vol.% does not result in strong variations of the 580.43 nm intensity. For higher addition (not shown), the quenching effect of oxygen became important and the post-discharge extinguished.

It can be seen in Fig. 3 that without any oxygen addition, the contact angle is 75° and that with the increase of the oxygen percentage, the contact angle regularly decreases to reach the lower limit of the contact angle measurement apparatus (i.e. below 5°) at 0.47% of O₂. This cannot be only explained by the evolution of the N(⁴S) concentration since it is almost constant from run S2 to run S5. Although N(⁴S) is considered as the main active species in pure nitrogen post-discharge, the introduction of oxygen in the discharge results in the creation of species such as O₂ in vibrationally and electronically excited states and O atomic radicals [38]. These species can react with silane and initiate chain reactions which can lead to deposition or to the formation of dust particles [39]. One could then expect the observation of oxygen emission lines. Nevertheless,

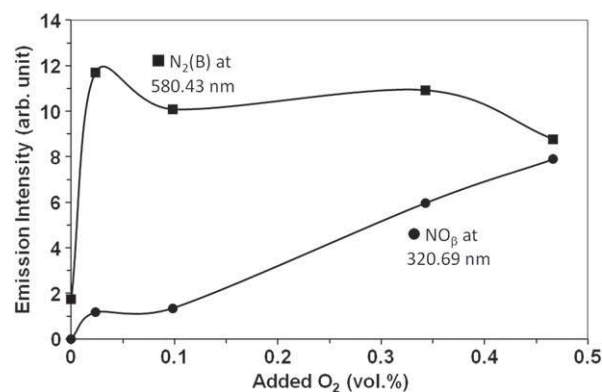


Fig. 4. Evolution of the emission intensity of the 580.43 nm (■) and 320.69 nm (●) as a function of the amount of added oxygen. These measurements were carried out just below the gas distributor with all the gas flowing through the distributor.

oxygen lines and especially the 777-nm line are not observed in the OES spectra of this study. This is not necessarily in contradiction with the possible presence of a small amount of atomic oxygen. Indeed, based on the chemical mechanism for NO titration methods in post-discharge described in Ref. [36] which is given in the reactions below, the NO_β state is due to O reacting with $\text{N}(^4\text{S})$ and a third body M (reaction (R4)).



Once NO in its ground state is obtained from NO_β deexcitation (reaction (R5)), it can react with $\text{N}(^4\text{S})$ to produce N_2 and O (reaction (R6)), as long as $\text{N}(^4\text{S})$ is available. $\text{N}(^4\text{S})$ can then react once again with O and so on ... When the amount of atomic oxygen reaches sufficient values, this steady state is broken due to high $\text{N}(^4\text{S})$ consumption and then NO radicals react with O instead of $\text{N}(^4\text{S})$ to produce $\text{NO}_2(\text{A})$ (reaction (R7)) with a characteristic green emission at 524 nm (reaction (R8)) which is not observed in our spectra. That is concomitant with vanishing of the 320-nm NO_β emission. So, as long as there are simultaneously NO and $\text{N}(^4\text{S})$, O is also present in the post-discharge and the NO_β 320-nm emission is observed. So the NO_β can be considered as a signature of the presence of atomic oxygen in the post-discharge. One can note that $\text{NO}(\text{X})$ can also be produced by the reactions of N_{2v} and $\text{N}_2(\text{A})$ with O [36]. In this context, from the clear increase of the NO_β 320-nm emission shown in Fig. 4, it can be concluded that the presence of oxygen in its reactive forms (excited and radical) is at the origin of the wettability improvement.

In order to understand the origin of the contact angle variation, the surface of the treated powders was analyzed by different means as described below.

First, the chemical bonds present at and near the powder surface were analyzed by ATR FT-IR. Fig. 5 presents the ATR FT-IR spectra before treatment and after runs S2 and S5. The spectrum obtained for the non-treated powders is identical to that observed in the literature for PE [40]. The two most important peaks at 2920 and

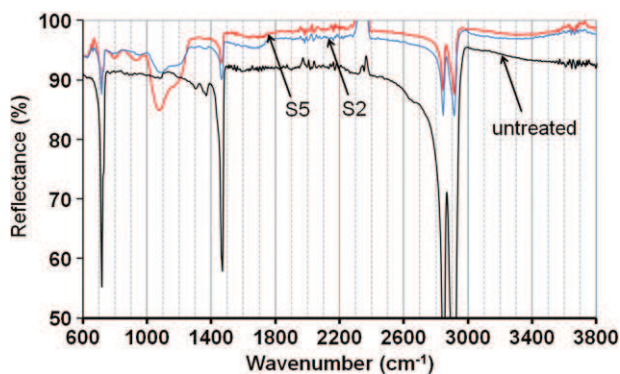


Fig. 5. FTIR-ATR spectra of the PE powders before and after deposition for runs S2 and S5.

2852 cm^{-1} can respectively be attributed to asymmetrical and symmetrical elongations of C-H in CH_2 . The two less important peaks at 1466 and 723 cm^{-1} are due to the deformation of C-H in $(\text{CH}_2)_n$ for the first one, and to the rocking of C-C in $(\text{CH}_2)_n-$ for the second one.

After deposition, the positions of the absorption peaks are quite similar for all the tested conditions. The spectra for S2 and S5 samples present IR absorptions at 1070 cm^{-1} , 800 cm^{-1} and 940 cm^{-1} which are typical of hydrogenated silicon oxide. They are respectively due to the vibrational stretching and bending modes of Si-O-Si groups and to Si-OH groups. The broad band between 3100 and 3500 cm^{-1} could be due to associated Si-OH groups at 3450 cm^{-1} . The presence of H_2O molecules at 3230 cm^{-1} and NH groups at 3330 cm^{-1} is also possible [41,42]. It is noteworthy that the 850 cm^{-1} vibration which is typical of silicon oxynitride is always absent from the spectra. This does not necessarily mean that during the process, no nitrogen atoms are included in the deposited film. Indeed, when silicon nitride is deposited at low temperature, it oxidizes toward silicon oxide producing ammonia [43]. The strong ammonia smell of the samples obtained with the lowest oxygen flow rates makes us think that such a post-oxidation of N-containing layers occurred [43].

From these FTIR analyses, it can be concluded that the origin of the wettability evolution shown in Fig. 3 is not linked to a variation of the deposit chemical composition. Nevertheless, it is worth noting that the intensity of the characteristic FTIR peaks of PE decreases relatively to that of the silicon oxide peaks when the oxygen flow rate increases. This could be due either to an increase of the deposition thickness or to a higher surface coverage by the deposit.

In order to visualize the surface of treated powders, FEG SEM analyses were performed before treatment and after runs S2 and S5, as illustrated in Fig. 6. The PE surface before deposition is quite smooth (Fig. 6a). The pattern on the untreated PE powders shown in Fig. 6b under high magnification is due to the platinum metallization which is required to avoid charge effects during SEM analyses. The surface of the treated powders (Fig. 6c and d) looks much more inhomogeneous as if dust particles had partially covered the powders. The number of particles is clearly more important for S5 than for S2. In Fig. 6e obtained under higher magnification, it can be seen that these dust particles present a cauliflower-like structure and also that they are deposited on or embedded in a film which itself presents a cauliflower-like structure. These observations are similar to those of Borer et al. [44] in a process where silicon oxide is deposited from hexamethyldisiloxane and oxygen on silica gel powders in a circulating fluidized bed reactor. According to their discussion, such a structure results from the low surface mobility of adatoms at low temperature. So, the nodular structure of the deposit and dusts which we observed is due to low temperature processing.

In order to estimate how the deposit covers the PE powders surface, EDX measurements were performed on various zones of samples from runs S2 and S5. All of the spectra shown in Fig. 7 present 3 clear peaks corresponding to C (0.277 keV), O (0.523 keV) and Si (1.74 keV). Another peak at 2.051 keV is due to Pt which is used for sample metallization.

All the spectra taken on run S5 samples are identical to Fig. 7a spectrum. The repeatability of these measurements and the large intensity of the Si and O radiations are the signature of a uniform deposition over the powder surface.

In the case of run S2 powders, depending on the localization of the measurement, two kinds of spectra were obtained, as illustrated in Fig. 7b and c. In Fig. 7b corresponding to zone B in Fig. 6c, silicon and oxygen lead to significant peaks, whereas in Fig. 7c corresponding to zone A in Fig. 6c, the intensities corresponding to both these species are much lower compared to that of carbon. Since the characteristic size of the analyzed zone by EDX is about 1 μm , i.e. much less than the surface of a single PE particle, we can just assert

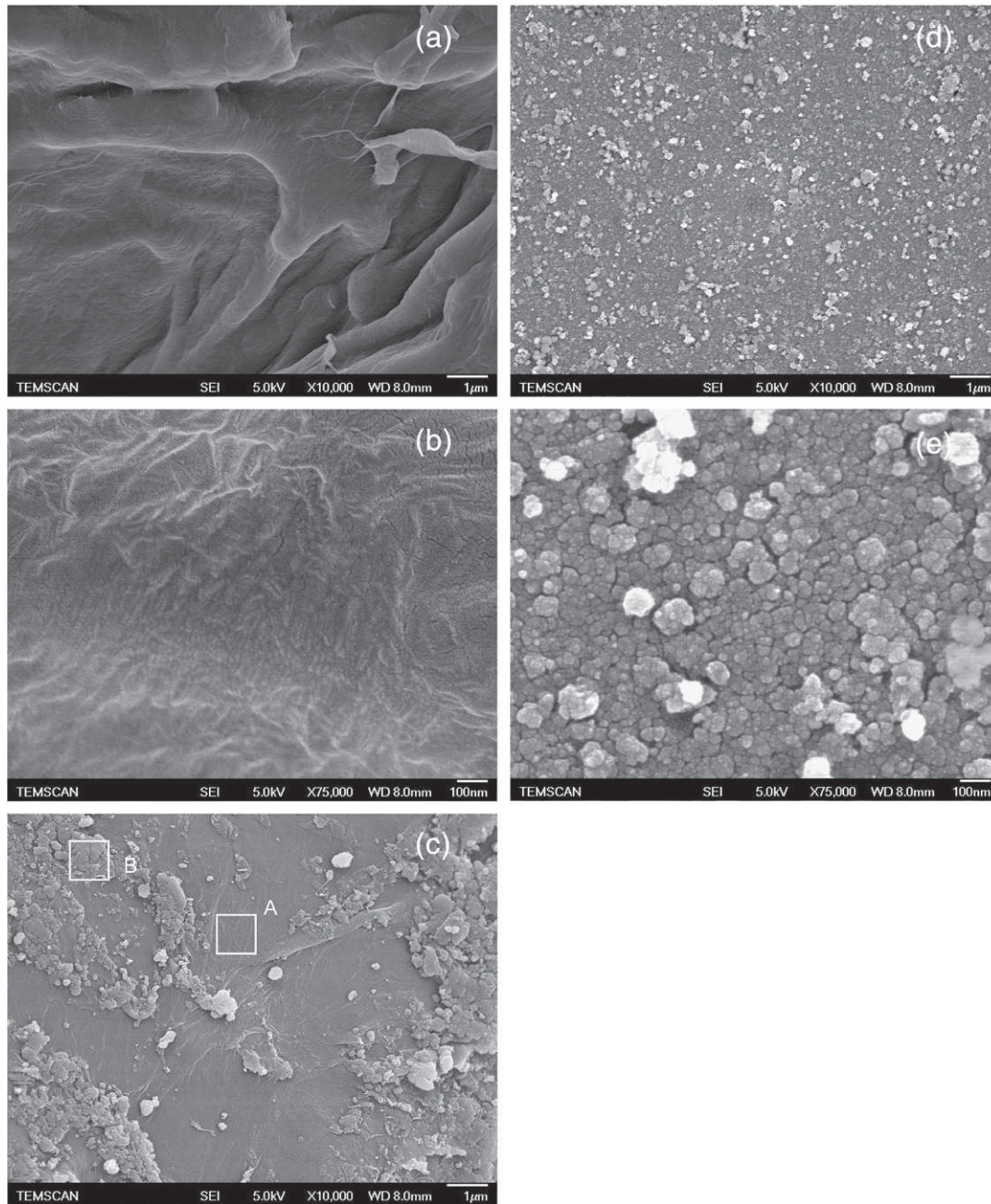


Fig. 6. FEG-SEM micrographs of the PE powder surface before deposition (a, b) after run S2 (c) and after run S5 (d, e). (b) and (e) are taken under magnification higher than (a), (c) and (d).

that we found places on run S2 powders which are poor in Si and O whereas such places were not found on run S5 powders. So, the qualitative trend is that whereas run S5 powders are uniformly covered by a silicon-oxide thin layer, run S2 powders are only partially covered. As PE is hydrophobic, this trend can explain the variations of the contact angle. The very low contact angle obtained for run S5 is then due to the complete coverage of the powders by a low contact angle silicon oxide (for instance, the contact angle of quartz is 38° [45]) and to the presence of silanol groups at the surface. So, depending on the operating conditions, the growth process can lead either to discontinuous coated zones or to a complete coverage of the powder. Based on these results, a first proposal for the deposition process can be drawn: the powder coating could occur via the creation of nucleation sites on the PE surface which initiate the growth of the layer. Then depending on the importance of these nucleation and growth phenomena, the powder is partially or

completely covered. Simultaneously, dust particles form and grow in the gas phase. They either stick to the column wall, or are embedded in the growing layer, or are carried out by the gas flow. A comparison between the spectra in Fig. 7 shows that between the C and O peaks the curve decreases to a low level in Fig. 7a whereas it remains relatively high in Fig. 7b which corresponds to the covered zone B (Fig. 6). This can be attributed to the presence of N atoms at 0.392 keV in Fig. 7b. Since Si-N peaks do not appear in ATR FT-IR spectra, the nitrogen atoms are probably underneath the film surface. The much lower N signal in Fig. 7a may be the result of the higher oxygen content of the gas. Indeed, atomic oxygen and nitrogen can both graft on polymer surfaces and etch them. During the one hour pre-treatment, nitrogen grafts on the powder surface. At the beginning of the treatment, oxygen is introduced and a competition between nitrogen-grafting and oxygen-grafting occurs. When the oxygen content increases, this competition leans towards oxygen

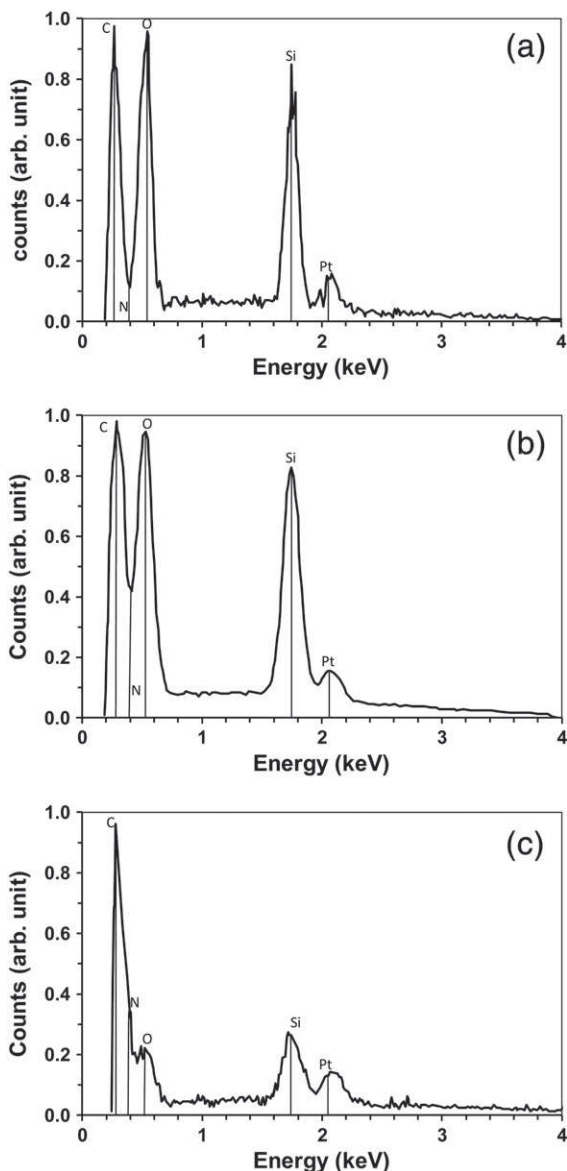


Fig. 7. EDX spectra for run S5 (a) and run S2 (b, c). Wherever the measurements were carried out for run S5 powders, similar results to (a) were obtained. In the case of run S2, depending on the measurement place, the spectrum can be similar to that of (b) or (c).

grafting and etching. So, for the highest tested oxygen concentration, the deposition essentially occurs on an oxygen-grafted surface, whereas nitrogen remains trapped under the deposit at lower oxygen concentration. So, this means that the state of the powder surface during the first few minutes of deposition changes with the oxygen concentration. Oxygen etching generally results in a modification of the surface roughness of polymers and this may influence the promotion of the nodular growth of the film as suggested by Borer et al. [46]. So, it is possible that the roughness increase due to oxygen etching results in a higher number of nucleation sites for the heterogeneous deposition of silicon oxide on the powder surface, whereas the less numerous nucleation sites obtained at lower oxygen concentrations results in an incomplete covering of the powders.

3.4. Aging

Although aging of plasma-treated polymers is well-described in the literature [47], only few papers studied the aging influence on powders [19,20]. The results of our aging study on runs S2 and S5

powders under ambient air are presented in Fig. 8. There is a clear increase of the contact angle with the storing time for both samples. Especially for run S5, the contact angle quickly rises from very low values and stabilizes at about 50°. This evolution could be due to the spreading of a hydrophobic carbonaceous contamination-layer on the silicon oxide film, as demonstrated by Ross et al. [45]. In their case, the aging of quartz after ion implantation was studied. The advancing contact angle of quartz samples treated by an Ar⁺ beam under an oxygen partial pressure is below 5° just after treatment and stabilized at about 50° after aging. This contact angle for aged quartz is the same as the one for aged run S5 sample. The aging of run S2 sample can be explained by the same way for its coated part.

3.5. Influence of the treatment duration

Knowing the specific surface area of powders ($0.0249 \text{ m}^2 \cdot \text{g}^{-1}$), a calculation based on the 0.18 g deposited mass during run S5 corresponds to a thin film thickness of 140 nm assuming that the deposit is amorphous silica (with a density of $2.2 \text{ g} \cdot \text{cm}^{-3}$) and uniform over the powder surface. The assumption of a uniform deposition is coherent with the repeatability of the EDX measurements on the surface of run S5 samples. Then, if the deposition were uniform all the run long, the film thickness would have been 70 nm for the one-hour run S8. Such a thickness would have been enough to reach the same wettability as the 140-nm thick layer given that the ATR-FTIR peaks are the same for runs S5 and S8 samples. So, the higher contact angle measured for run S8 (Table 2) is probably the consequence of a discontinuity of the deposit on the powder surface. This is in agreement with the proposal for a nucleation and growth mechanism: the shorter S8 duration leads to the creation of fewer nucleation sites and to a smaller growth of the coating from these nucleation sites finally leading to uncovered zones.

3.6. Influence of the silane flow rate

When 2 sccm of silane is injected at the bed bottom (run S7 in Table 2) instead of 4 (run S5), the chemistry certainly leads to lower nucleation rates and the deposit growth from the nucleation sites is slower. As a consequence, after run S7, the expanding islands probably do not merge leaving a part of the powder uncovered. Then, although ATR-FTIR peaks are the same as in run S5 (not shown), the water contact angle is only 42.5°.

4. Conclusion

In the present work, temperature-sensitive polyethylene (PE) powders were successfully coated by silicon oxide in a fluidized bed

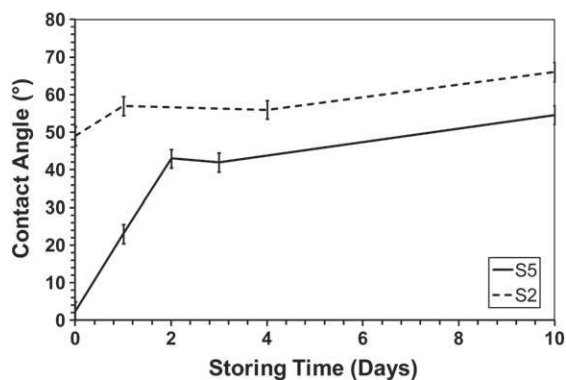


Fig. 8. Variation of the water contact angle as a function of storing time for runs S2 (dashed line) and S5 (plain line).

placed in a far cold remote nitrogen/oxygen plasma at temperatures lower than 100 °C.

Depending on the operating conditions, the wettability improvement varies from bad to very good. Based on ATR FT-IR, FEG-SEM, and EDX analyses, it is proposed that the film deposition occurs via nucleation and growth of nodules on the PE surface. Simultaneously, dust particles form and grow in the gas phase and they can be either embedded in the growing layer or carried out by the gas flow. The intensity of these phenomena varies with the operating parameters, which can lead to incomplete surface coverage. This allows explaining first the nodular structure of the deposited film and also the variations of the water contact angle depending on the oxygen and silane concentrations and the treatment duration. When the experimental conditions did not lead to the merging of the growing nodules, the water wettability is not as good as when the powder is completely covered by a silicon oxide film.

Acknowledgments

The authors would like to acknowledge *M. Molinier* from LGC/INPT for his precious technical assistance. This study was performed thanks to a PRES PhD grant of Toulouse University and a Bonus Qualité Recherche funding from Paul Sabatier University.

References

- [1] S.M. Rosnagel, W.D. Westwood, J.J. Haber, *Handbook of Plasma Processing Technology: Fundamental, Etching, Deposition and Surface Interactions*, William Andrew, Norwich, 1991.
- [2] C. Xu, J. Zhu, *Chem. Eng. Sci.* 60 (2005) 6529.
- [3] N. Célini, F. Bergaya, F. Poncin-Epaillard, *Polymer* 48 (2007) 58.
- [4] D. Shi, J. Lian, P. He, L.M. Wang, W.J. van Ooij, M. Schulz, Y. Liu, D.B. Mast, *Appl. Phys. Lett.* 81 (2002) 5216.
- [5] C. Bayer, M. Karches, A. Matthews, P.R. von Rohr, *Chem. Eng. Technol.* 21 (1998) 427.
- [6] S.H. Park, S.D. Kim, *Colloids Surf. A* 133 (1998) 33.
- [7] M. Tatoulian, F. Brétagnot, F. Arefi-Khonsari, J. Amouroux, O. Bouloussa, F. Rondelez, A.J. Paul, R. Mitchell, *Plasma Process. Polym.* 2 (2005) 38.
- [8] P.R. von Rohr, B. Borer, *Chem. Vap. Deposition* 13 (2007) 499.
- [9] J. Pichal, J. Hladik, P. Spatenka, *Plasma Process. Polym.* 6 (2009) 148.
- [10] A. Sonnenfeld, A. Spillmann, C. Arpagaus, P. Rudolf von Rohr, *Plasma Process. Polym.* 6 (2009) 170.
- [11] M. Karches, C. Bayer, P.R. von Rohr, *Surf. Coat. Technol.* 116–119 (1999) 879.
- [12] C. Vivien, C. Wartelle, B. Mutel, J. Grimblot, *Surf. Interface Anal.* 34 (2002) 575.
- [13] J.B. Leroy, N. Fatah, B. Mutel, J. Grimblot, *Plasma Polym.* 8 (2003) 13.
- [14] V. Guerra, P.A. Sa, J. Loureiro, *Eur. Phys. J. Appl. Phys.* 28 (2004) 125.
- [15] R. D'Agostino, P. Favia, C. Oehr, M.R. Wertheimer, *Plasma Process. Polym.* 2 (2005) 7.
- [16] S.H. Jung, S.H. Park, S.D. Kim, *J. Chem. Eng. Jpn.* 37 (2004) 166.
- [17] I. Loh, R.E. Cohen, R.F. Baddour, *J. Appl. Polym. Sci.* 31 (1986) 901.
- [18] S.H. Jung, S.H. Park, D.H. Lee, S.D. Kim, *Polym. Bull.* 47 (2001) 199.
- [19] C. Arpagaus, A. Rossi, P. Rudolf von Rohr, *Appl. Surf. Sci.* 252 (2005) 1581.
- [20] F. Brétagnot, M. Tatoulian, F. Arefi-Khonsari, G. Lorang, J. Amouroux, *React. Funct. Polym.* 61 (2004) 221.
- [21] L. Aiche, H. Vergnes, B. Despax, B. Caussat, H. Caqueneau, *Interface Controlled Organic Thin Films*, Springer, Berlin Heidelberg, 2009, p. 79.
- [22] K. Teshima, Y. Inoue, H. Sugimura, O. Takai, *Surf. Coat. Technol.* 169–170 (2003) 583.
- [23] S. Vallon, *Thin Solid Films* 290–291 (1996) 68.
- [24] E.W. Washburn, *Phys. Rev.* 17 (1921) 273.
- [25] P. Supiot, O. Dessaux, P. Goudmand, *J. Phys. D: Appl. Phys.* 28 (1995) 1826.
- [26] S. Bockel, A.M. Diemy, A. Ricard, *Surf. Coat. Technol.* 74–75 (1995) 474.
- [27] P. Merel, M. Tabbal, M. Chaker, M. Moisan, A. Ricard, *Plasma Sources Sci. Technol.* 7 (1998) 550.
- [28] J.-P. Sarrette, B. Rouffet, A. Ricard, *Plasma Process. Polym.* 3 (2006) 120.
- [29] S. Villegier, M. Sixou, J. Durand, A. Ricard, *J. Phys. D: Appl. Phys.* 39 (2006) 3826.
- [30] M.F. Llop, F. Madrid, J. Arnaldos, J. Casal, *Chem. Eng. Sci.* 51 (1996) 5149.
- [31] L. Aiche-Belkadi, *Modification des propriétés de surface de poudres en lit fluidisé assisté par une post-décharge*, PhD Thesis, University of Toulouse, France, 2009 (http://thesesups.ups-tlse.fr/693/1/Aiche-Belkadi_Lynda.pdf).
- [32] J.F. Davidson, D. Harrison, *Fluidised Particles*, Cambridge University Press, 1963.
- [33] A.E. Wraith, R. Harris, *Miner. Eng.* 5 (1992) 993.
- [34] C. Hollenstein, *Plasma Phys. Control. Fusion* 42 (2000) R93.
- [35] B. Gordiets, C. Ferreira, V. Guerra, J. Loureiro, J. Nahorny, D. Pagnon, M. Touzeau, M. Vialle, *IEEE Trans. Plasma Sci.* 23 (1995) 750.
- [36] M.K. Boudam, B. Saoudi, M. Moisan, A. Ricard, *J. Phys. D: Appl. Phys.* 40 (2007) 1694.
- [37] J. Nahomy, C.M. Ferreira, B. Gordiets, D. Pagnon, M. Touzeau, M. Vialle, *J. Phys. D: Appl. Phys.* 28 (1995) 738.
- [38] M. Mrázková, P. Vasina, V. Kudrle, A. Talsky, C.D. Pintassilgo, V. Guerra, *J. Phys. D: Appl. Phys.* 42 (2009) 075202.
- [39] K.D. Bleecker, D. Herrebout, A. Bogaerts, R. Gijbels, P. Descamps, *J. Phys. D: Appl. Phys.* 36 (2003) 1826.
- [40] J.V. Gulmine, P.R. Janissek, H.M. Heise, L. Akcelrud, *Polym. Test.* 21 (2002) 557.
- [41] A. Brunet-Bruneau, J. Rivory, B. Rafin, J.Y. Robic, P. Chaton, *J. Appl. Phys.* 82 (1997) 1330.
- [42] G. Dupont, H. Caqueneau, B. Despax, R. Berjoan, A. Dollet, *J. Phys. D: Appl. Phys.* 30 (1997) 1064.
- [43] J.N. Chiang, S.G. Ghanayem, D.W. Hess, *Chem. Mater.* 1 (1989) 194.
- [44] B. Borer, A. Sonnenfeld, P. Rudolf von Rohr, *Surf. Coat. Technol.* 201 (2006) 1757.
- [45] G.G. Ross, M. Chass, M. Bolduc, *J. Phys. D: Appl. Phys.* 36 (2003) 1001.
- [46] B. Borer, R. von Rohr, *Surf. Coat. Technol.* 200 (2005) 377.
- [47] M. Ataefard, S. Moradian, M. Mirabedini, M. Ebrahimi, S. Asiaban, *Plasma Chem. Plasma Process.* 28 (2008) 377.